End-to-end simulation of high-contrast imaging systems: methods and results for the PICTURE mission family

Ewan S. Douglas, Kuravi Hewawasam, Christopher B. Mendillo, Kerri L. Cahoy, Timothy A. Cook, et al.

Ewan S. Douglas, Kuravi Hewawasam, Christopher B. Mendillo, Kerri L. Cahoy, Timothy A. Cook, Susanna C. Finn, Glenn A. Howe, Marc J. Kuchner, Nikole K. Lewis, Anne D. Marinan, Dimitri Mawet, Supriya Chakrabarti, "End-to-end simulation of high-contrast imaging systems: methods and results for the PICTURE mission family," Proc. SPIE 9605, Techniques and Instrumentation for Detection of Exoplanets VII, 96051A (16 September 2015); doi: 10.1117/12.2187262

SPIE.

Event: SPIE Optical Engineering + Applications, 2015, San Diego, California, United States

End-to-end simulation of high-contrast imaging systems - methods and results for the PICTURE mission family

Ewan S. Douglas[a], Kuravi Hewawasam[b], Christopher B. Mendillo[b], Kerri L. Cahoy[c,d], Timothy A. Cook[b], Susanna C. Finn[b], Glenn A. Howe[b], Marc J. Kuchner[f], Nikole K. Lewis[g], Anne D. Marinan[c], Dimitri Mawet[e,h], Supriya Chakrabarti[b]

[a]Astronomy Department, Boston University, Boston, MA, USA 02215;
[b]Lowell Center For Space Science and Technology, UMASS Lowell, Lowell, MA, USA 01854;
[c]Department of Aeronautics and Astronautics, Massachusetts Institute of Technology, Cambridge, MA, USA 02139;
[d]Department of Earth and Planetary Science, Massachusetts Institute of Technology, Cambridge, MA, USA 02139;
[e]Jet Propulsion Laboratory, California Institute of Technology, Pasadena, CA, USA 91125;
[f]NASA Goddard Space Flight Center, Greenbelt, MD, USA 20771;
[g]Space Telescope Science Institute, Baltimore, MD, USA 21218;
[h]Astronomy Department, California Institute of Technology, Pasadena, CA, USA 91125.

ABSTRACT

We describe a set of numerical approaches to modeling the performance of spaceflight high-contrast imaging payloads. Mission design for high-contrast imaging requires numerical wavefront error propagation to ensure accurate component specifications. For constructed instruments, wavelength and angle-dependent throughput and contrast models allow detailed simulations of science observations, allowing mission planners to select the most productive science targets. The PICTURE family of missions seek to quantify the optical brightness of scattered light from extrasolar debris disks via several high-contrast imaging techniques: sounding rocket (the Planet Imaging Concept Testbed Using a Rocket Experiment) and balloon flights of a visible nulling coronagraph, as well as a balloon flight of a vector vortex coronagraph (the Planetary Imaging Concept Testbed Using a Recoverable Experiment - Coronagraph, PICTURE-C). The rocket mission employs an on-axis 0.5m Gregorian telescope, while the balloon flights will share an unobstructed off-axis 0.6m Gregorian. This work details the flexible approach to polychromatic, end-to-end physical optics simulations used for both the balloon vector vortex coronagraph and rocket visible nulling coronagraph missions. We show the preliminary PICTURE-C telescope and vector vortex coronagraph design will achieve 10^{-8} contrast without post-processing as limited by realistic optics, but not considering polarization or low-order errors. Simulated science observations of the predicted warm ring around Epsilon Eridani illustrate the performance of both missions.

1. INTRODUCTION

Space-based instruments for high-contrast imaging of exoplanets and debris disks operate at the cutting edge of optical manufacturing where subtle changes in the wavefront error (WFE), orders of magnitude smaller than typical ground-based adaptive optics residuals, have large influences on the science yield. We are currently preparing two high-contrast imaging missions for upcoming flights in 2015, 2017 and 2019, both of which provide insight into pertinent design and modeling factors. The first is a sounding rocket experiment, named PICTURE (Planet Imaging Concept Testbed Using a Rocket Experiment), is expected to launch in Fall 2015 and image the Epsilon Eridani (ϵ-Eridani) circumstellar environment for approximately 210 seconds. The second, a stratospheric balloon named PICTURE-C (Planetary Imaging Concept Testbed Using a Recoverable Experiment - Coronagraph), is scheduled to launch twice, once in Fall 2017 and in Fall 2019. In addition to re-observing ϵ-Eridani, PICTURE-C

Further author information: (Send correspondence to E.S.D or K.H.)
E.S.D.: E-mail: douglase@bu.edu; KH: E-mail: kuravi_hewawasam@student.uml.edu

Techniques and Instrumentation for Detection of Exoplanets VII, edited by Stuart Shaklan, Proc. of SPIE Vol. 9605
96051A · © 2015 SPIE · CCC code: 0277-786X/15/$18 · doi: 10.1117/12.2187262

will measure the visible light circumstellar environments of other nearby stars with large infrared excess.[1] The PICTURE sounding rocket is an 0.5 m on-axis Gregorian telescope equipped with an active pointing system and a visible nulling coronagraph (VNC) built around a 32x32 actuator microelectromechanical system deformable mirror (MEMS DM).[2,3] The PICTURE-C balloon[1] will fly an off-axis 0.6m afocal Gregorian telescope and a low order wavefront correction system. The first balloon flight includes the PICTURE VNC, while the second flight will use a vector vortex coronagraph[4] (VVC) coupled with an microwave kinetic inductance detector[5] (MKID) with design goal of achieving in-flight instrument contrasts of order 10^{-7}. As space-based, high-contrast, coronagraphic missions with ambitious science goals, both require high-fidelity simulation of coronagraph performance in order to quantify the expected science yield. In some respects the modeling approaches of the two missions have differed significantly. For example, much attention has been given to prediction of the count rates for the brief PICTURE sounding rocket observation, while great care has gone into a diffraction propagation modeling of PICTURE-C to ensure deep contrast.

Prior space-based astronomical observatories have used lightweight PSF modeling libraries for simulating science results both before and after launch.[6,7] Maximizing the science return of missions requires careful management of design parameters, subtle decisions regularly face the instrument designer, such as trade-offs between wavefront error at different spatial frequencies, or the signal-to noise ratio change from switching to potentially less uniform, but more reflective, coating. Similar trade-offs present themselves to the observer, for example the choice between a distant star with a relatively bright dust ring versus a higher contrast dust ring around a nearby star. Computationally efficient modeling of such subtle effects, in a robust and repeatable manner, allows easy tracking of expected science yield versus manufacturing realities. Expensive commercial software packages aimed at the optical engineer provide important information for the system mechanical layout and tolerancing, but would be unnecessarily complicated for specification of optical quality and science result simulation. Our approach is to generate flexible models of the telescope and coronagraph using diffraction-based optical models in programming languages commonly used for data analysis, such as IDL or Python, thereby minimizing the divide between instrument engineering and the final science product.

The PICTURE team's approach to modeling the final instrument contrast and PSF is shown in Fig. 1. First an astronomical target is defined and the expected target spectrum is combined with the system spectral response using the *pysynphot* Python package.[8] A wavefront of the appropriate wavelength, tilt, and intensity is then propagated through a diffraction model, which is defined by the coronagraph and telescope opto-mechanical design. Previous numerical simulations for high-contrast ground-based[9] and proposed spaceflight systems[10] have used the the *PROPER*[11] package written in IDL for Fresnel wavefront propagation. For the PICTURE-C modeling of a vector vortex coronagraph and speckle suppression, we have built on the publicly available work of the NASA ROSES Technology Development for Exoplanet Missions (TDEM) reports comparing internal coronagraphs, the reports will subsequently be referred to as TDEM1[12] and TDEM2.[13] For sounding rocket telescope and VNC modeling we employ the Fraunhofer diffraction tools found in the Physical Optical Propagation in Python module (*POPPY*[7]). The final complex wavefront provides an input to a simulated wavefront sensor for further correction of the coronagraph model, and as an input to a science camera model where appropriate plate scale and noise are applied. The end-to-end sequence is repeated for a set of wavelengths spanning the science band, the intensities of which are determined by the output of the *pynsynphot* spectral modeling. For modeling stellar systems with multiple targets (exoplanets) or resolved targets (debris disks), this entire process is repeated over a set of wavefronts simulating a set of incoherent sources. While processor intensive, running each wavefront through such a propagation system, which includes a coronagraph model, ensures the coronagraph throughput and target PSF(s) are representative of our best understanding of the system.

PICTURE-C mission design and observation planning is ongoing and this work presents a snapshot of efforts to date. We illustrate our mission simulation with a combination of both missions in the PICTURE family. We demonstrate our approach while sharing the PICTURE-C design performance to the extent that it has been quantified to date. Following the flow of Fig. 1, we will first discuss modeled stellar spectra and instrument throughput. We will next define the optical surfaces for diffraction modeling and discuss the operation of both the PICTURE VNC and VVC coronagraphs. Finally, we will present the application of wavefront propagation libraries to simulating broadband, end-to-end science observations using the PICTURE payloads.

Figure 1: Overview of high-contrast imaging payload modeling. Relevant software packages used are indicated by square brackets. Depending on the instrument design, the science detector and the Wavefront Sensor (WFS) detector may use separate detectors (as in the PICTURE VNC) or a single image plane detector (as in the PICTURE-C Vector Vortex + MKID design).

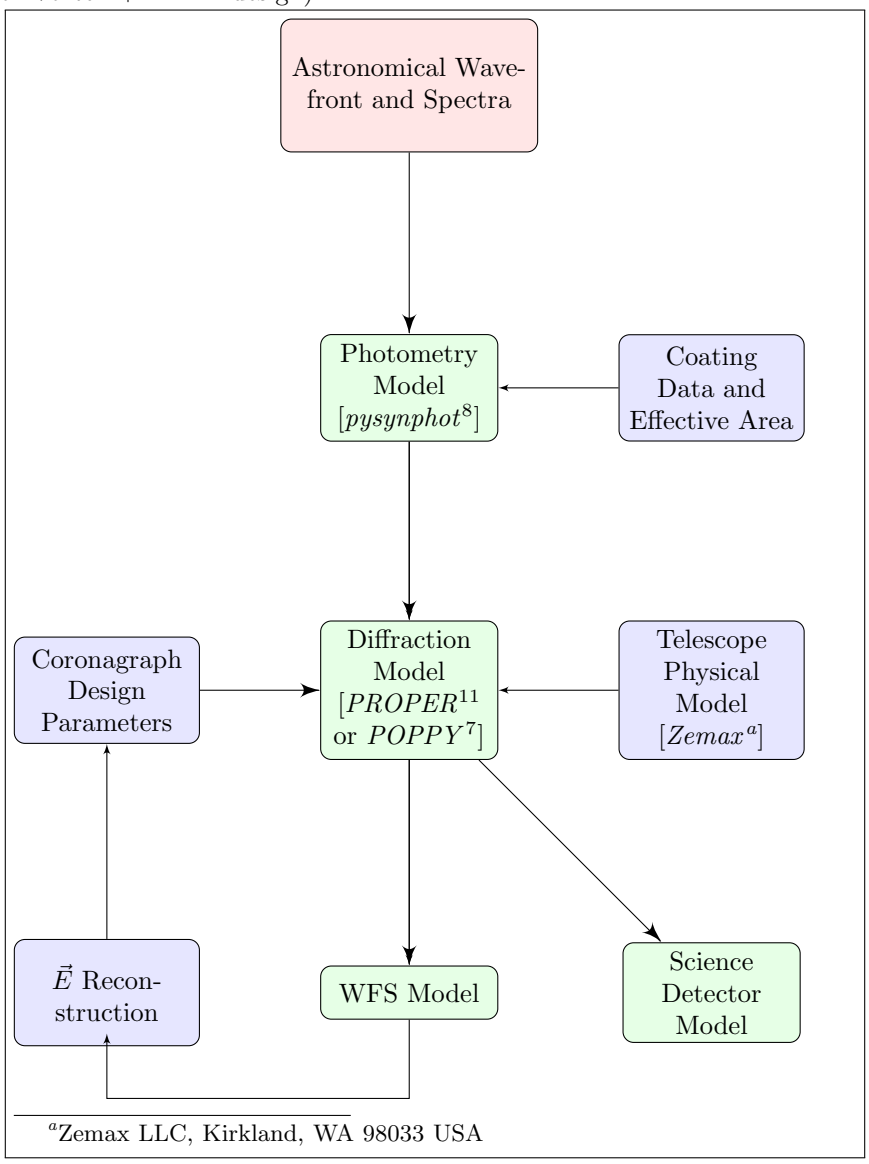

2. METHODS

2.1 Spectral Throughput

Accurate spectral throughput models illustrate the wavelength dependence of point spread functions and speckles and provide realistic inputs for wavefront correction simulations. Additionally, to model signal-to-noise ratios, photon rates are required and the target star visible magnitude provides flux calibration of the model spectra. The *pysynphot* synthetic photometry package[8] is used to generate input spectra from a empirical stellar flux library.[14] Using *pysynphot*'s interpolation and unit conversion functions, bandpasses are generated by multiplying by the responses of the spectral throughput of each element. These modeled responses include protected silver, gold and antireflection coatings and detector quantum efficency for each type of surface preceeding the output of each detector. These are applied to the input stellar spectra, as illustrated in Fig. 2, for a B8I spectral-type star,

which closely approximates Rigel, the planned calibration target of the PICTURE sounding rocket flight. Curves are shown for a blue band (below 6000 Å) which feeds the angle tracker (AT) to maintain payload pointing[15] and for the science band (6000-7500 Å). The decreased detector quantum efficiency and coating reflectivity at short wavelengths combine for a dramatic decrease in photons measured at the angle tracker, shown in the modeled curve, versus a flat, system response of unity.

Figure 2: Example of using *pysynphot* to generate synthetic spectra for speckle modeling and count rate predictions. Modeled responses accounting for coating transmission and quantum efficiency are shown opposed to a flat 100% throughput for a B8I star, the short wavelength band (< 6000Å) corresponds to the PICTURE sounding rocket angle tracker camera (AT). The science band (6000-7500Å) is also shown, indicating the number of photons reaching the pupil imaging wavefront sensor (WFS).

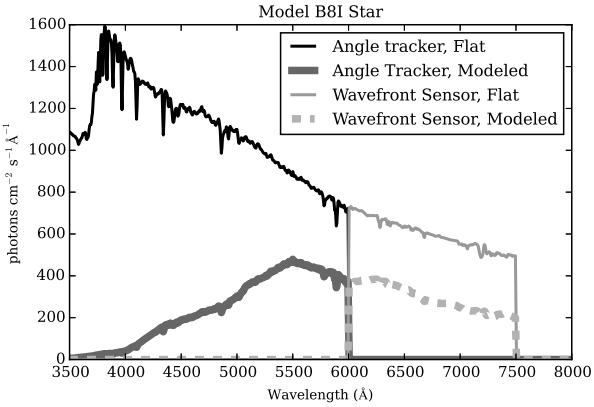

2.2 Wavefront Error

WFE propagation routines such as *PROPER* and *POPPY* provide the means to simulate the propagation of a wavefront through an optical system. The afocal telescope design for the PICTURE-C experiment is modeled by the 18 elements given in Tables 1 and 2, arranged as shown in Fig. 3. Optical details of the sounding rocket payload telescope and VNC are detailed in Rao et al[2] and Mendillo et al.[3] For the purpose of simulation each system is configured in a linear fashion (all elements normal to the beam).

2.2.1 Surface Error

In order to model an physical optics system, manufacturing errors of the optical elements must be taken in to account. Wavefront aberrations due to the surface irregularities of each element of the system are essential to any simulation that hopes to predict actual measurements. TDEM2[13] provides a basic framework to model the effect of these irregularities of the surface and reflectance of each component. An irregularity on the surface of a mirror (due to figuring and polishing) will imprint a phase error on a wavefront, while an irregularity in the reflectance (due to coating variations) will imprint an amplitude error. This is modeled by applying synthetic two-dimensional error maps to the wavefront phase and amplitude. These maps are generated from random realizations of error maps which follow the power spectral density (PSD) curve given by Eq. 1, which was derived from measurements of actual optics in TDEM2. The parameters a, b, and c used for subsequent simulations are given in Table 2 for each optic.

$$PSD = \frac{a}{\left(1 + (k/b)^2\right)^{c/2}} \tag{1}$$

All generated surface maps are saved at the time of model initialization as FITS Files for later retrieval. Fig. 4 shows an instance of the surface map of the primary mirror (M1) generated as described along with the ideal one-dimensional PSD of the surface and a measurement of a random realization used for simulation. Similar to

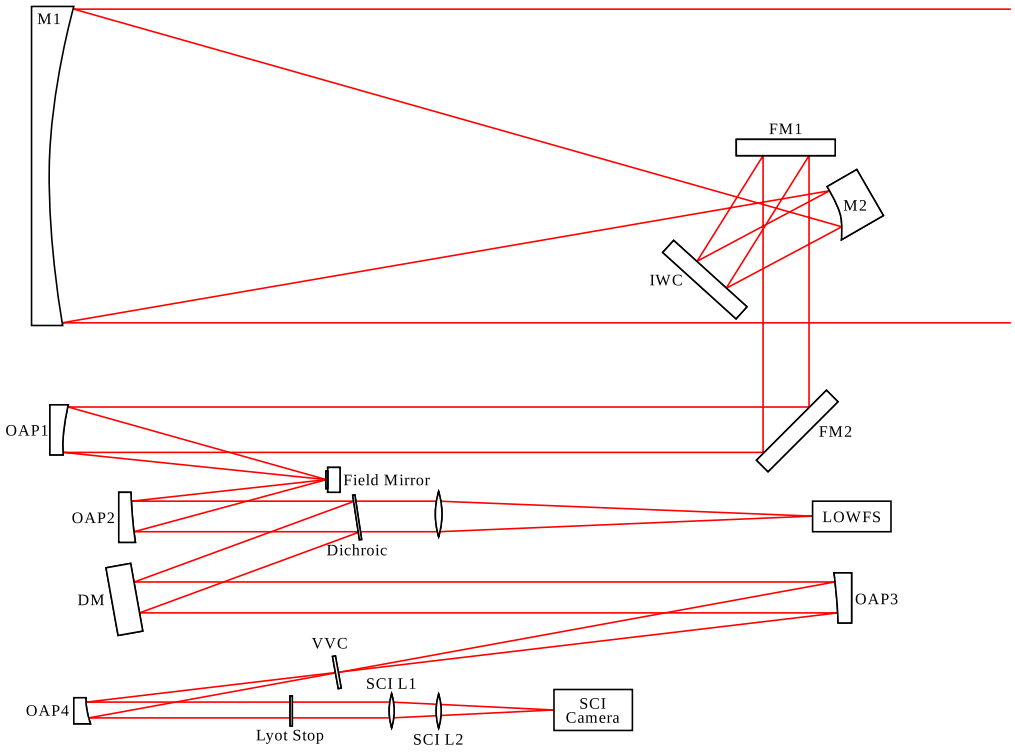

Figure 3: Flattened schematic diagram of the PICTURE-C telescope and vector vortex coronagraph optical system. Note that the telescope is un-obstructed and the optics shown in the primary ray path are off-axis. A schematic of the PICTURE sounding rocket optical system can be found in Mendillo et al.[3]

TDEM2, a cut-off of 32 cycles/aperture (twice the Nyquist frequency of a 32x32 DM) is also applied to the PSD to avoid numerical errors at higher spatial frequencies caused by the Fourier transforms used in the propagations.

For the sounding rocket VNC payload, instead of modeling each element, individual components of the VNC are specified as $< \lambda/20$ peak-to-valley (PV) surface figure and their contribution to wavefront error at correctable spatial frequencies is assumed to be negligible compared to intensity mismatch, whereas the primary mirror (M1) is of order $\lambda/4$ PV surface figure. Thus, the M1 figure has an outsized contribution to the wavefront error (WFE) through the system. These low spatial frequency components of the M1 surface contribute a phase mismatch to the nuller which is correctable by the MEMS deformable mirror. Uncorrected spatial frequency errors (> 15 cycles/aperture) scatter light to larger angles and define the outer working angle. At twice the control frequency, the DM exhibits highly-correlated print through[2] at the actuator frequency. Since the DM only corrects the difference between the two effective apertures, all spatial frequencies of the primary mirror surface contribute to the post-coronagraph PSF. This decreases sensitivity to dim companions independent of the nuller effectiveness by increasing the size of a resolution element, lowering the per-pixel companion signal, and increasing the proportion of unattenuated star-light away from the PSF core.

2.2.2 Amplitude Error

Reflectance maps are created in the same manner and applied to the waveform as a modification to its amplitude. At the moment, the same form of PSD (Eq. 1) is used, but additional forms of non-uniformity of the optical coating may be specified. Figure 5 shows an instance of the reflectance map of the primary mirror generated as described along with the one dimensional PSD of the reflectance.

Table 1: Optical prescription for PICTURE-C system. Abbreviations used: M indicates powered mirrors, the LOWFS is the low order wavefront sensor, FM indicates fold mirrors, the IWC is the integrated wavefront controller, and OAPs are off-axis-parabolas.

Name	Focal length [in]	Distance to the next optic [in]	Radius [in]
M1	60	64.32	12
M2	4.32	4.63	1
IWC	0	7	0.89
FM1	0	75	1
FM2	0	26	1
OAP1	10.5	10.5	1
Field	−0.9	7.33	1
OAP2	7.33	9	1
Dichroic	0	10.5	1
DM	0	28	0.62
OAP3	20	20	1
VVC	0	10	0.5
OAP4	10	8	1
Lyot Stop	0	4	0.27
SCI Lens 1	4.32	4	1
SCI Lens 2	4.32	4	1
SCI Camera	0	0	0

Table 2: PSD parameters used to generate the synthetic amplitude and surface error maps for the PICTURE-C PROPER model. FS is fused silica.

	Surface				Reflectivity					
Name	PV [nm]	RMS [nm]	b [1/m]	c	PV [%]	RMS [%]	b [1/m]	c	Coating	Material
M1	60	8	10	4	7	1	10	4	AlSiO	none
M2	30	5.5	10	4	2.5	0.5	10	4	AgSiO	none
IWC	30	5.5	10	4	2.5	0.5	10	4	AgSiO	none
FM1	30	5.5	10	4	2.5	0.5	10	4	AgSiO	none
FM2	30	5.5	10	4	2.5	0.5	10	4	AgSiO	none
OAP1	30	5.5	10	4	2.5	0.5	10	4	AgSiO	none
Field	30	5.5	10	4	2.5	0.5	10	4	AgSiO	none
OAP2	30	5.5	10	4	2.5	0.5	10	4	AgSiO	none
Dichroic	30	5.5	10	4	2.5	0.5	10	4	Dichroic	FS
DM	30	5.5	10	4	2.5	0.5	10	4	AuSiO	none
OAP3	30	5.5	10	4	2.5	0.5	10	4	AgSiO	none
OAP4	30	5.5	10	4	2.5	0.5	10	4	AgSiO	none
SCI Lens 1	30	5.5	10	4	2.5	0.5	10	4	none	FS
SCI Lens 2	30	5.5	10	4	2.5	0.5	10	4	none	FS

Figure 4: Error map (left) and one-dimensional PSD (right) of simulated surface non-uniformity of the PICTURE-C primary mirror (M1), the functional form of the surface PSD used as input is shown as a solid line and the PSD measured from the generated two-dimensional surface is shown as a dashed line.

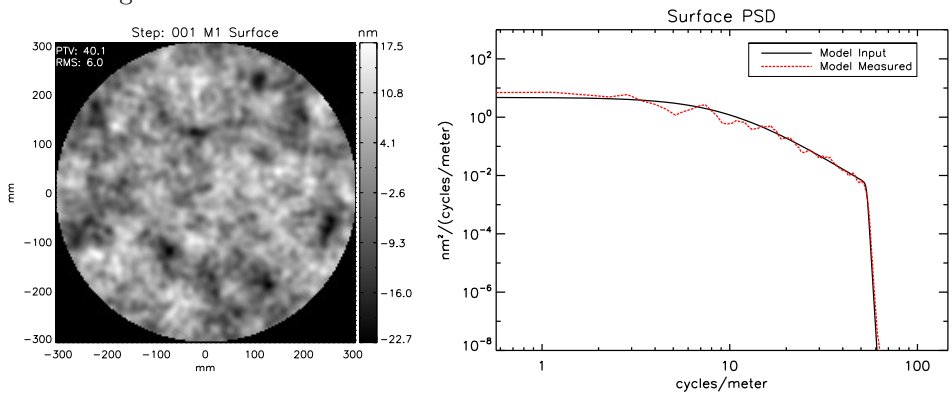

Figure 5: Error map (left) and one-dimensional PSD (right) of simulated reflectivity non-uniformity of the PICTURE-C primary mirror (M1), the functional form of the PSD used as input is shown as a solid line and the PSD measured from the generated two-dimensional surface is shown as a dashed line.

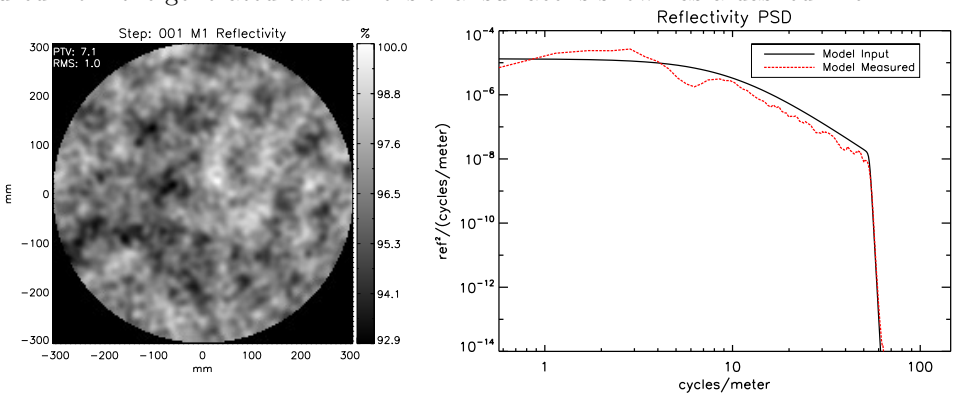

For simplicity, in subsequent simulations of the PICTURE VNC sounding rocket payload, rather than model each optic, an assumed interferometer arm intensity mismatch of 5% provides a first order approximation of coronagraph performance.

3. CORONAGRAPHS

3.1 Visible Nulling Coronagraph

Visible nulling coronagraphs (VNCs) employ destructive interference to block starlight from the image plane while transmitting light from small angular separations, revealing exoplanets and debris disks.[16–18] The PICTURE VNC applies a lateral shear to a copy of the telescope pupil, generating two sub-apertures separated by a distance analogous to a radio interferometer's baseline. The two pupil copies have a relative π phase shift, generating a fringe pattern which depends on angle on the sky. In order to maximize null depth, mid-to-low spatial frequency mismatches in relative path length are corrected by a 32x32 Boston Micromachines Inc. MEMS DM. The design has achieved in-lab white light attenuation of simulated starlight of approximately 10^{-4} at the inner working angle ($1.7\lambda/D$).

While an understanding of Fresnel diffraction effects is important for high-contrast imaging, in the PICTURE VNC the intra-instrument propagation beam covers a short distance, is masked at the edges, and operates in a mid-contrast regime ($\approx 10^{-3}$). Therefore, Fraunhofer propagation from instrument pupil plane to the science camera approximates first order system performance – useful for the purpose of determining the influence of telescope and deformable mirror surface quality on the science goals.

3.2 Vector Vortex Coronagraph

A Vector Vortex is a liquid crystal polymer based optical element that introduces an azimuthally-varying phase shift (a geometrical phase spiral) to the wavefront.[4] Applying a vector vortex at an image plane normal to incoming starlight creates a beam with a phase spiral and a central singularity, causing self-interference in the planar wavefront which generates a dark central region in the downstream beam. In a VVC, this effect is exploited by placing a Lyot stop at the corresponding pupil plane. The TDEM coronagraph comparison report, TDEM1, contains an extensively-modeled ideal vector vortex. We employed this framework for the VVC to simulate the performance of the PICTURE-C system.

4. DIFFRACTION MODEL RESULTS

4.1 Sounding Rocket Simulations

To quantify the influence of the PICTURE sounding rocket telescope surface error on the science image, we assume a simple VNC model where the dominant sources of surface error are the telescope and DM surfaces, capturing both the highly correlated DM signal and the aberrated telescope surface. Both are placed in pupil planes allowing a simple Fraunhofer diffraction model to simulate WFE propagation to the instrument PSF. Using *POPPY*, an complex input wavefront is sheared, and the DM surface error at uncorrectable spatial frequencies is optionally added to one arm. After the beams are combined, a binary transmission Lyot mask applied to block regions where the two pupils do not overlap and the complex wavefront is multiplied by the sheared telescope complex wavefront error, simulating correction of relative, but not absolute, WFE between the interferometer arms. The left two columns of Fig. 6 show the variation in phase and amplitude of ideal (top) and extremely astigmatic (bottom) example interfered post-Lyot wavefronts. From this final pupil plane, Fraunhofer propagation is carried out for each wavefront. The third column of of Fig. 6 shows the wavefront difference at the image plane for each case, corresponding to the interferometer dark output, while the right-most column shows the bright output PSF.

To simulate a realistic source, a single bright wavefront with zero tilt (a central star) and a set of lower amplitude tilted wavefronts (composing a number of faint companion sources, N_S) are individually propagated through a simple nuller model for a number of wavelength bins (N_λ). After propagation to the image plane, each wavefront is added incoherently. This process is repeated at each wavelength of interest. *POPPY* implements the Matrix Fourier Transform,[19] which does not require equal array sizes in the pupil, and permits significant speed gains when a small number of focal plane pixels is required relative to the sampling of the pupil plane. If the propagation time per wavefront is t_p the total simulation time is $t_P \times N_\lambda \times N_S = 615 t_p$. For a 1024x1024 pupil array and a 132x132 pixel image, oversampled 10×, and $N_\lambda = 15$, $N_S = 41$ on a Core i5 laptop processor t_p is of order five seconds. Thus, such a simulation requires nearly an hour of processing time. However, since each wavefront is independent, the problem was parallelized via the *IPython IPCluster* module.[20] The total processing time for such a set of 615 wavefronts is approximately 4.4 minutes using a 40 node IPCluster, across 20 physical E5-2670 Intel Xenon(R) Cores at 2.50 GHz at the Boston University Shared Computer Cluster. Decreasing the image plane array size to sample only the central 35 pixels, oversampled to 345x345, decreases simulation time to 1.3 minutes.

4.2 Simulated Sounding Rocket VNC Science Image

Nearby and dusty, the ϵ-Eridani system has one of the brightest known debris disks, making it an ideal target to demonstrate high-contrast imaging in a short-duration observation. We illustrate the PICTURE payload expected science results in Fig. 7a using a simple model of the inner warm debris disk from Backman et al:[21] a face-on ring, of radius one arcsecond, with infinitesmal thickness, and an integrated brightness of $2 \times 10^{-4} L_\star$. Fig. 7b shows a final science image with idealized speckle subtraction. The count rate and stellar color are approximated using *pysynphot* as described previously. This model shows the that the $\lambda/4$ low-spatial frequency surface figure of the sounding rocket primary will recover the predicted debris disk.

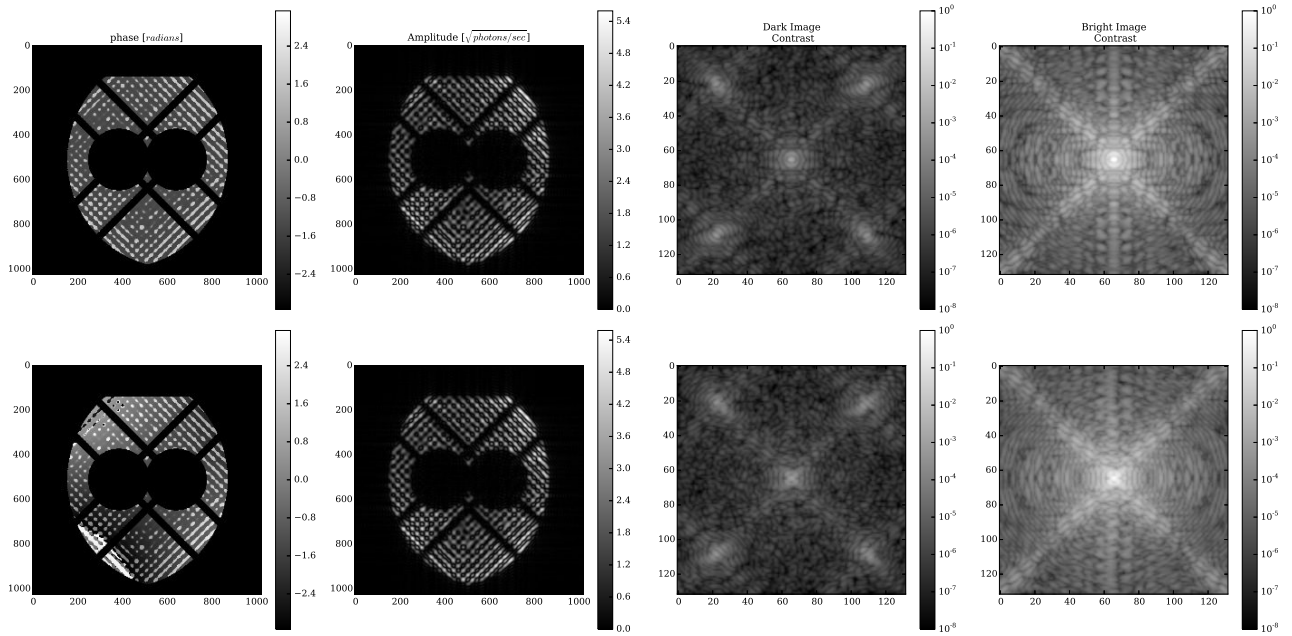

Figure 6: Example simulation of monochromatic interference for the sounding rocket telescope with a realistic uncorrectable deformable mirror surface print through and intensity leakage. The leftmost column shows the pupil plane phase (without unwrapping) in radians after interfering the two complex wavefronts. The second column shows the dark output amplitude, the third column shows a focal plane image of the science camera contrast in the dark fringe output, and the rightmost column shows the corresponding bright fringe output. The top row corresponds to an ideal telescope and the lower row corresponds to an astigmatic telescope with an unacceptable 280 nm of PV surface astigmatism. The contrast or distribution of leaked starlight is slightly changed without changing the total and the telescope Strehl ratio, seen in the bright fringe, decreases with the addition of this (unrealized) amount of astigmatism.

4.3 VVC Simulation

For the extreme high-contrast imaging regime of the proposed PICTURE-C VVC, Fresnel diffraction effects from each element must be considered. Once initialized by generating the optical surfaces and errors enumerated in Tables 1 and 2, a final image is simulated using plane-to-plane wavefront propagation[22] through the complete system. For the examples presented here we employed PROPER 2.0*. Fig. 8a shows the resultant contrast map for a broadband (550-660 nm) simulation of PICTURE-C, using Electric Field Conjugation (EFC[23]), to dig a so-called "dark hole" on the right side of the image plane. Within the dark hole, the modeled contrast exceeds 10^{-8} assuming ideal electric field sensing in the image plane. The contrast map shown corresponds to the final dark hole generated from the PICTURE-C prescription with a radius of 10 λ/d generated after 30 EFC iterations. Fig. 8b shows that the dark hole contrast started below 10^{-3}, then a phase flattening using the electric field at the occulter focal plane decreases the average to below 10^{-5} and provides the starting point for the EFC algorithm which brings the mean contrast to below 10^{-8} after approximately 15 iterations.

For EFC, the electric field response at the detector for each DM actuator is simulated. Each actuator of the DM is poked and a flat wavefront is propagated through the system to find the electric field at the detector. These electric field measurements are used to generate the DM response matrix. The simulated focal plane image is then used to solve the inverse problem of finding the DM pattern that minimizes the energy inside a specified dark hole. For a broadband system, the inverse problem is solved simultaneously for multiple wavelengths. Detailed descriptions of the phase flattening process and EFC algorithms employed here are given in TDEM1 and TDEM2.

*`http://sourceforge.net/projects/proper-library/`

Figure 7: Simulated 210 second sounding rocket observation of the predicted inner warm ring of ϵ-Eridani[21] using the PICTURE VNC, a $\lambda/4$ surface figure primary telescope, the flight deformable mirror, and a 5% intensity mismatch between the interferometer arms. Deformable mirror print through errors at the actuator frequency can be see as four bright spikes defining the outer working angle. Poisson, detector dark, and detector read noise are included.

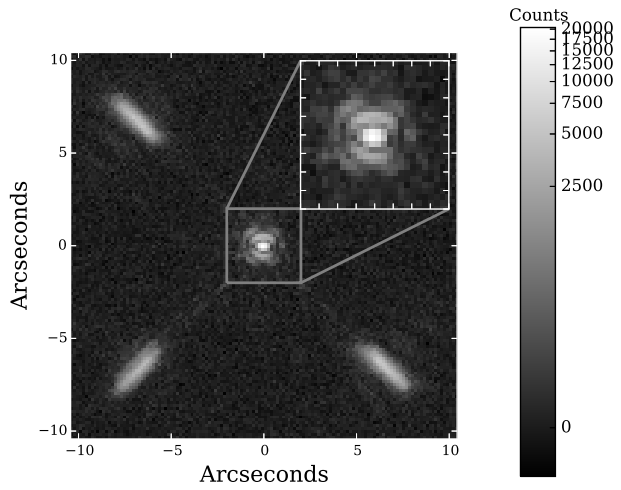

(a) Simulated average image as will be recorded during the PICTURE sounding rocket flight. The debris disk is nearly lost in the wings of the leaking PSF.

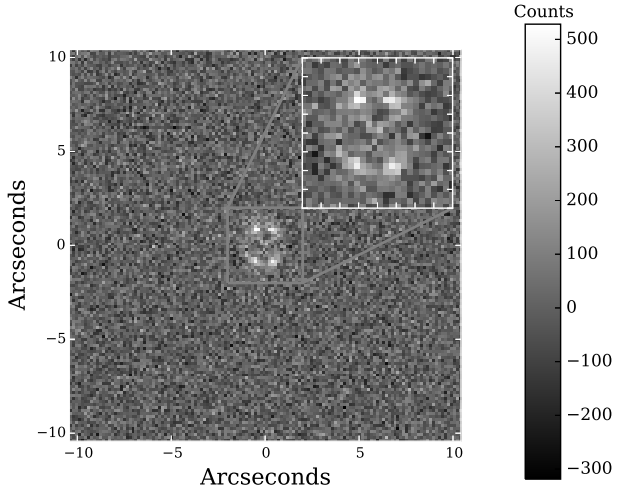

(b) After ideal PSF subtraction only noise and the predicted inner ring are visible. The expected face on ring is truncated at zero and 1" by the vertically oriented nuller fringe pattern. Speckle subtraction will be enabled by measurement of a calibration star and by a mid-observation spacecraft roll during the ϵ-Eridani observation.

4.4 Simulated PICTURE-C VVC Science Contrast

Fig. 9a illustrates the PICTURE-C balloon exected performance for the simple ϵ-Eridani disk model used previously in this work for sounding rocket simulations. Fig. 9b shows the an equivalent simulation without the dust ring. This example is broadband but does not yet include a *pysynphot* generated spectrum, photon noise, or time dependent variations such as beam walk, pointing errors and payload gravity vector rotation.

5. CONCLUSIONS

We have described a framework and a toolbox of software packages for end-to-end modeling of the PSFs and science images of high contrast imaging systems. We have illustrated how various tools have been used for decision making during the design and mission planning phases of two suborbital high-contrast missions – the PICTURE sounding rocket and the PICTURE-C stratospheric balloon. Efforts are ongoing to incorporate all aspects of modeling into a single software architecture, particularly extending the POPPY physical optics modeling package to the Fresnel regime.

Work is in-progress to generate simulated sciences images for the rest of the PICTURE-C target list . Future modeling will include errors due to dust, time-dependent varitions and uncertainty in electric field retrieval in the EFC routine. The current PICTURE-C system performance exceeds the contrast post-processing design goal of 10^{-7} by more than a factor of ten without post-processing. Thus, the design is expected to have sufficient margin to absorb these un-modeled influences.

6. ACKNOWLEDGEMENTS

This work was funded by NASA grants NNG05WC17G, NNX11AD53G, and NNX15AG23G and through graduate fellowships awarded to E.S. Douglas by the Massachusetts Space Grant Consortium. Special thanks to

Figure 8: Preliminary PICTURE-C PROPER modeling results including surface and reflectivity errors and DM correction.

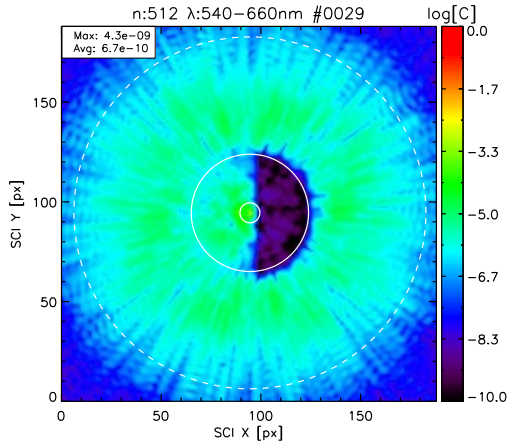

(a) PICTURE-C broadband image plane contrast map showing the contrast provided by the VVC and a dark hole created by thirty iterations of EFC. This contrast map corresponds to the simulated science image corrected for spatial variations in VVC transmission divided by the peak pixel value of a simulation of the same system with the VVC element removed.[12]

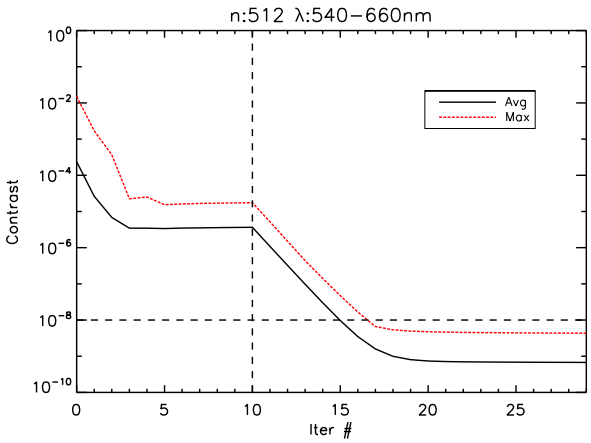

(b) Simulated time series of PICTURE-C broadband contrast convergence versus EFC iterations. The mean contrast within the dark hole is shown as a solid line, while the brightest speckle in the dark hole is shown as a dashed line.

Figure 9: Preliminary simulation of PICTURE-C balloon observation in units of contrast for an observation of the same predicted dust ring shown in 7b, this simulation does not include an observation duration, thus photon noise is neglected.

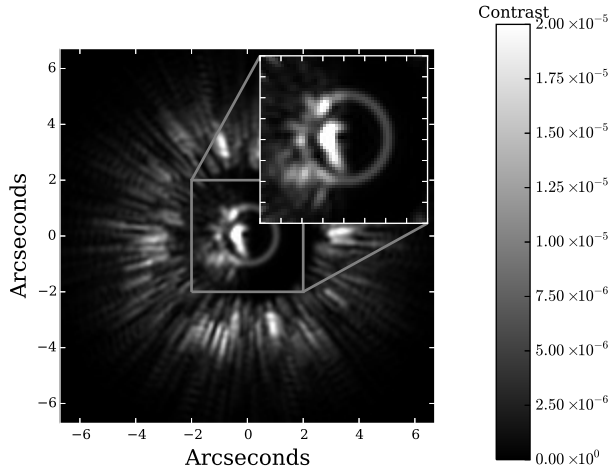

(a) Raw PICTURE-C telescope and VVC simulation with end-to-end broadband model of the ϵ-Eridani warm-inner ring.[21] Compared to the sounding rocket VNC payload the outer working angle is smaller. However, more of the disk is resolved due to the higher system Strehl ratio and coronagraph contrast.

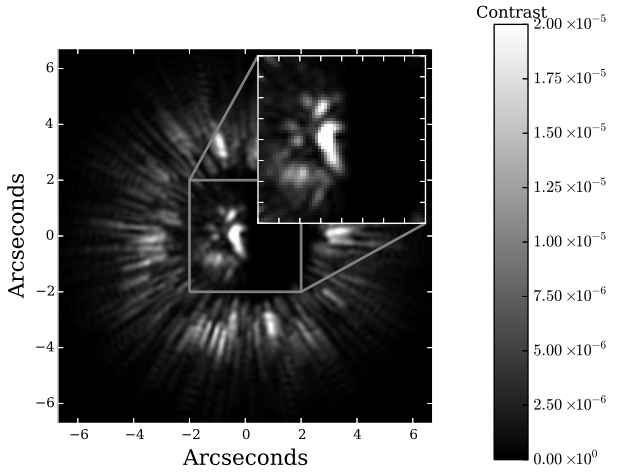

(b) Comparison image of the same optical system without a dust ring showing the residual speckle pattern after EFC correction. As an alternative to the half-focal plane dark hole shown, a symmetrical circular dark hole could be created at the expense of average contrast or outer working angle.

Brian Hicks for many helpful conversations. Measurements of telescope mirror reflectivities provided by ISP Optics and typical reflectivities provided by Thorlabs. This research made use of Astropy,a community-developed

core Python package for Astronomy;[24] the IPython Interactive Computing architecture;[20] IDL (Exelis Visual Information Solutions, Boulder, Colorado); and the SIMBAD database, operated at CDS, Strasbourg, France.

REFERENCES

1. Cook, T., Cahoy, K. L., Chakrabarti, S., Douglas, E., Finn, S., Kuchner, M., Lewis, N., Marinan, A., Martel, J., Mawet, D. P., Mazin, B., Mendillo, C. B., Serabyn, E., Stuchlik, D., and Swain, M., "Planetary Imaging Concept Testbed Using a Recoverable Experiment - Coronagraph (PICTURE – C)," *JATIS* **Submitted** (2015).
2. Rao, S. R., Wallace, J. K., Samuele, R., Chakrabarti, S., Cook, T., Hicks, B., Jung, P., Lane, B., Levine, B. M., Mendillo, C., Schmidtlin, E., Shao, M., and Stewart, J. B., "Path length control in a nulling coronagraph with a MEMS deformable mirror and a calibration interferometer," in [*Proc. SPIE*], **6888**, 68880B–68880B (Feb. 2008).
3. Mendillo, C. B., Hicks, B. A., Cook, T. A., Bifano, T. G., Content, D. A., Lane, B. F., Levine, B. M., Rabin, D., Rao, S. R., Samuele, R., Schmidtlin, E., Shao, M., Wallace, J. K., and Chakrabarti, S., "PICTURE: a sounding rocket experiment for direct imaging of an extrasolar planetary environment," in [*Proc. SPIE*], **8442** (Sept. 2012).
4. Mawet, D., Serabyn, E., Liewer, K., Burruss, R., Hickey, J., and Shemo, D., "The Vector Vortex Coronagraph: Laboratory Results and First Light at Palomar Observatory," *ApJ* **709**, 53 (Jan. 2010).
5. Mazin, B. A., Bumble, B., Meeker, S. R., OBrien, K., McHugh, S., and Langman, E., "A superconducting focal plane array for ultraviolet, optical, and near-infrared astrophysics," *Optics Express* **20**, 1503 (Jan. 2012).
6. Krist, J., "Simulation of HST PSFs using Tiny Tim," in [*ASPC IV*], **77**, 349 (1995).
7. Perrin, M. D., Soummer, R., Elliott, E. M., Lallo, M. D., and Sivaramakrishnan, A., "Simulating point spread functions for the James Webb Space Telescope with WebbPSF," in [*Proc. SPIE*], **8442**, 84423D–84423D–11 (2012).
8. STScI development Team, "pysynphot: Synthetic photometry software package," *Astrophysics Source Code Library,* **ascl:1303.023** (2013).
9. Marois, C., Macintosh, B., Soummer, R., Poyneer, L., and Bauman, B., "An end-to-end polychromatic Fresnel propagation model of GPI," in [*Proc. SPIE*], **7015**, 70151T (July 2008).
10. Krist, J. E., Belikov, R., Pueyo, L., Mawet, D. P., Moody, D., Trauger, J. T., and Shaklan, S. B., "Assessing the performance limits of internal coronagraphs through end-to-end modeling: a NASA TDEM study," in [*Proc. SPIE*], **8151**, 81510E–81510E–16 (2011).
11. Krist, J. E., "PROPER: an optical propagation library for IDL," in [*Proc. of SPIE*], **6675**, 66750P–66750P–9 (2007).
12. Krist, J. E., Belikov, R., Mawet, D. P., Moody, D., Pueyo, L., Shaklan, S. B., and Trauger, J. T., "Technology Milestone 1 Results Report: Assessing the performance limits of internal coronagraphs through end-to-end modeling," Tech. Rep. JPL Document D-74425, JPL (2013).
13. Krist, J. E., Belikov, R., Mawet, D. P., Moody, D., Pueyo, L., Shaklan, S. B., and Trauger, J. T., "Technology Milestone 2 Results Report: Assessing the performance limits of internal coronagraphs through end-to-end modeling," Tech. Rep. JPL Document D-74426, JPL (2013).
14. Pickles, A., "A Stellar Spectral Flux Library: 115025000 ," *PASP* **110**, 863–878 (July 1998).
15. Mendillo, C. B., Chakrabarti, S., Cook, T. A., Hicks, B. A., and Lane, B. F., "Flight demonstration of a milliarcsecond pointing system for direct exoplanet imaging," *Applied Optics* **51**, 7069–7079 (Oct. 2012).
16. Bracewell, R. N., "Detecting nonsolar planets by spinning infrared interferometer," *Nature* **274**, 780–781 (Aug. 1978).
17. Angel, J. R. P. and Woolf, N. J., "An Imaging Nulling Interferometer to Study Extrasolar Planets," *ApJ* **475**, 373 (Jan. 1997).
18. Shao, M., Wallace, J. K., Levine, B. M., and Liu, D. T., "Visible nulling interferometer," in [*Proc. SPIE*], **5487**, 1296–1303 (Oct. 2004).
19. Soummer, R., Pueyo, L., Sivaramakrishnan, A., and Vanderbei, R. J., "Fast computation of Lyot-style coronagraph propagation," *Opt. Express* **15**, 15935–15951 (Nov. 2007).

20. Perez, F. and Granger, B., "IPython: A System for Interactive Scientific Computing," *Computing in Science Engineering* **9**, 21–29 (May 2007).
21. Backman, D., Marengo, M., Stapelfeldt, K., Su, K., Wilner, D., Dowell, C. D., Watson, D., Stansberry, J., Rieke, G., Megeath, T., Fazio, G., and Werner, M., "Epsilon Eridani's Planetary Debris Disk: Structure and Dynamics Based on Spitzer and Caltech Submillimeter Observatory Observations," *ApJ* **690**, 1522–1538 (Jan. 2009).
22. Lawrence, G. N., "Optical Modeling," in [*Applied Optics and Optical Engineering.*], Shannon, R. R. and Wyant., J. C., eds., **XI**, Academic Press, New York (1992).
23. Give'on, A., Kern, B., Shaklan, S., Moody, D. C., and Pueyo, L., "Broadband wavefront correction algorithm for high-contrast imaging systems," in [*Proc. SPIE*], **6691** (2007).
24. The Astropy Collaboration, Robitaille, T. P., Tollerud, E. J., Greenfield, P., Droettboom, M., Bray, E., Aldcroft, T., Davis, M., Ginsburg, A., Price-Whelan, A. M., Kerzendorf, W. E., Conley, A., Crighton, N., Barbary, K., Muna, D., Ferguson, H., Grollier, F., Parikh, M. M., Nair, P. H., Gnther, H. M., Deil, C., Woillez, J., Conseil, S., Kramer, R., Turner, J. E. H., Singer, L., Fox, R., Weaver, B. A., Zabalza, V., Edwards, Z. I., Azalee Bostroem, K., Burke, D. J., Casey, A. R., Crawford, S. M., Dencheva, N., Ely, J., Jenness, T., Labrie, K., Lim, P. L., Pierfederici, F., Pontzen, A., Ptak, A., Refsdal, B., Servillat, M., and Streicher, O., "Astropy: A community Python package for astronomy," *A&A* **558**, A33 (Oct. 2013).